

Cortical neural populations can guide behavior by integrating inputs linearly, independent of synchrony

Mark H. Histed¹ and John H. R. Maunsell

Department of Neurobiology, Harvard Medical School, Boston, MA 02115

Edited by Ranulfo Romo, Universidad Nacional Autónoma de México, Mexico City, D.F., Mexico, and approved November 25, 2013 (received for review October 8, 2013)

Neurons are sensitive to the relative timing of inputs, both because several inputs must coincide to reach spike threshold and because active dendritic mechanisms can amplify synchronous inputs. To determine if input synchrony can influence behavior, we trained mice to report activation of excitatory neurons in visual cortex using channelrhodopsin-2. We used light pulses that varied in duration from a few milliseconds to 100 ms and measured neuronal responses and animals' detection ability. We found detection performance was well predicted by the total amount of light delivered. Short pulses provided no behavioral advantage, even when they concentrated evoked spikes into an interval a few milliseconds long. Arranging pulses into trains of varying frequency from beta to gamma also produced no behavioral advantage. Light intensities required to drive behavior were low (at low intensities, channelrhodopsin-2 conductance varies linearly with intensity), and the accompanying changes in firing rate were small (over 100 ms, average change: 1.1 spikes per s). Firing rate changes varied linearly with pulse intensity and duration, and behavior was predicted by total spike count independent of temporal arrangement. Thus, animals' detection performance reflected the linear integration of total input over 100 ms. This behavioral linearity despite neurons' nonlinearities can be explained by a population code using noisy neurons. Ongoing background activity creates probabilistic spiking, allowing weak inputs to change spike probability linearly, with little amplification of coincident input. Summing across a population then yields a total spike count that weights inputs equally, regardless of their arrival time.

neuronal circuits | population coding | optogenetics | mouse

Many neurons in the brain receive thousands of inputs spread over their dendritic trees, and several of those inputs need to be active simultaneously to generate a spike reliably (1, 2). In this way, coincident synaptic inputs can be amplified relative to asynchronous inputs. In addition to this nonlinearity caused by spike threshold, other active processes such as dendritic calcium spikes (3–5) can preferentially amplify synchronous inputs. A variety of ways that timing could impact network function have been explored, including oscillatory synchronization (6, 7), strong cascading effects of individual neurons or synapses (8–11), and information encoding via temporal patterns (12). In the songbird, for example, song neurons receive precisely timed coincident input that recruits active calcium conductances, generating strong, reliable spike bursts that control the song (13, 14). However, synchrony might not always be critical for neuronal processing. Several types of models show that neuronal networks can be insensitive to precise spike timing even though individual neurons are highly sensitive. Most of these models rely on strong (15) or numerous (16–18) inputs and amplification of small perturbations, leading to chaotic network dynamics and noisy single neurons (15, 17, 19). Experimental data show that at times neuronal responses can combine responses to sensory input linearly, as with simple cells in visual cortex (20, 21). However, it has been unclear how either synchronous or linear responses in the cerebral cortex might guide behavior.

Determining how input synchrony influences behaviors requires both behavioral measurements and the ability to identify and record the neurons used for behavior. Optogenetic stimulation provides an opportunity to study the effects of synchrony, because it allows us to supply input to a restricted set of neurons and ask animals to make behavioral responses that depend on the activity of those neurons. Because each input spike results in a brief change in conductance in postsynaptic neurons, we can study the effects of synchrony by providing large transient changes in conductance or weaker sustained changes. These changes in conductance simulate the effects on single cells when their many presynaptic partners fire synchronously or asynchronously. Thus, we can study synchrony not by measuring correlated spiking in a large population of neurons, but by simulating the effects of an input population of varying synchrony by controlling conductance amplitude and duration.

Here, we trained mice to perform a behavioral task in which they monitored background activity in their visual cortex and reported when cells were stimulated optogenetically. This approach allowed us to provide conductance input to the neurons that drive the behavior, vary the strength and duration of the input, and measure how input synchrony affects behavioral performance. We find that animals' detection performance is predicted only by the total amount of light power delivered and not by its pattern within a 100-ms interval. Stimulation produces only small changes in the spiking of neurons and population responses vary linearly with pulse duration and amplitude. Thus, behavior is predicted by the total number of spikes fired above baseline, independent of their temporal pattern. Unexpectedly, cellular nonlinearities do not appear to be exploited to improve detection performance for synchronous input. Hereafter

Significance

The brain performs computations by transforming sensory inputs to make decisions. We study these neuronal computations in the mouse, one of the smallest animals with a cerebral cortex, the part of the human brain that controls complex behavior. We find animals' behavior can be insensitive to the timing of cortical inputs, depending only on total spike count, even though individual neurons are sensitive to timing. Thus, the cortex can integrate input linearly, or place equal weight on inputs regardless of their arrival time. This emergent linear network behavior may arise from fluctuations in membrane potential generated by background network activity. Brain diseases may arise from dysfunction of these network properties, perhaps by damaging the mechanisms that create this background noise.

Author contributions: M.H.H. and J.H.R.M. designed research; M.H.H. performed research; M.H.H. analyzed data; and M.H.H. and J.H.R.M. wrote the paper.

The authors declare no conflict of interest.

This article is a PNAS Direct Submission.

¹To whom correspondence should be addressed. E-mail: mark_histed@hms.harvard.edu.

This article contains supporting information online at www.pnas.org/lookup/suppl/doi:10.1073/pnas.1318750111/-DCSupplemental.

we use the term “synchronous input” to describe the brief, strong changes in conductance that we provide (and that are produced in single cells when input spikes arrive synchronously; shown schematically in Fig. 1A). However, because we observe linear spike responses, “synchronous” also can be used to describe spike patterns: We find that a constant number of evoked spikes produces the same behavioral detection performance, no matter whether spikes are arranged synchronously or are spread out over a 100-ms interval.

Results

Animals Reliably Report Changes in Neuronal Firing Induced by Channelrhodopsin-2. We stimulated a small region of primary visual cortex (V1) using channelrhodopsin-2 (ChR2). We limited expression to excitatory pyramidal neurons using a transgenic mouse (*Emx1-Cre*) and viral transfection. We illuminated a spot <1 mm in diameter on the surface of the exposed dura to stimulate hundreds to thousands of transfected neurons (Fig. 1C and Figs. S1 and S2), comparable to the number of neurons affected by the smallest possible visual stimulus because of the size and scatter of V1 receptive fields (22). Animals readily detected ChR2 stimulation, and we obtained precise psychometric thresholds for direct cortical stimulation, as in sensory tasks (23), by changing the intensity of the stimulus (Fig. 1D and E). Moving the excitation light to an adjacent area of cortex with weaker expression dramatically reduced animals' ability to do the task (Fig. 1F and Fig. S2), as would be expected if the animals

were directly detecting changes in neuronal activity and not the laser light. Shorter reaction times to cortical stimulation [~ 150 ms minimum compared with ~ 210 ms minimum in a visual task (23)] are further evidence that animals detect direct neuronal activation, as has been shown previously in a range of species and brain areas (24–28).

Detection Performance Varies with Total Stimulation Power. To examine the importance of input synchrony for behavior, we used different temporal patterns of excitation light to simulate synchronized or desynchronized synaptic input. We chose a 100-ms maximum interval to ensure that recorded neuronal responses were not contaminated by activity related to motor response or reward, because animals' reaction times could be as fast as 150 ms (Fig. 1E).

We first delivered short and long pulses of light, scaling pulse amplitude to find detection threshold, which is the amplitude that produces equal detection performance for each pulse duration (Fig. 2A). We found that detection threshold varied inversely with pulse duration, so when pulse duration was reduced by a factor of 10, the amplitude needed to achieve the same performance was increased by approximately a factor of 10. To eliminate any possibility that this variation could be influenced by fluctuation in perceptual criterion, we measured threshold both in terms of percent correct, corrected for false alarms (Methods and Fig. 2B–D; $n = 4$ animals, slope on a log–log plot of duration vs. threshold percent correct: mean -0.87 , largest

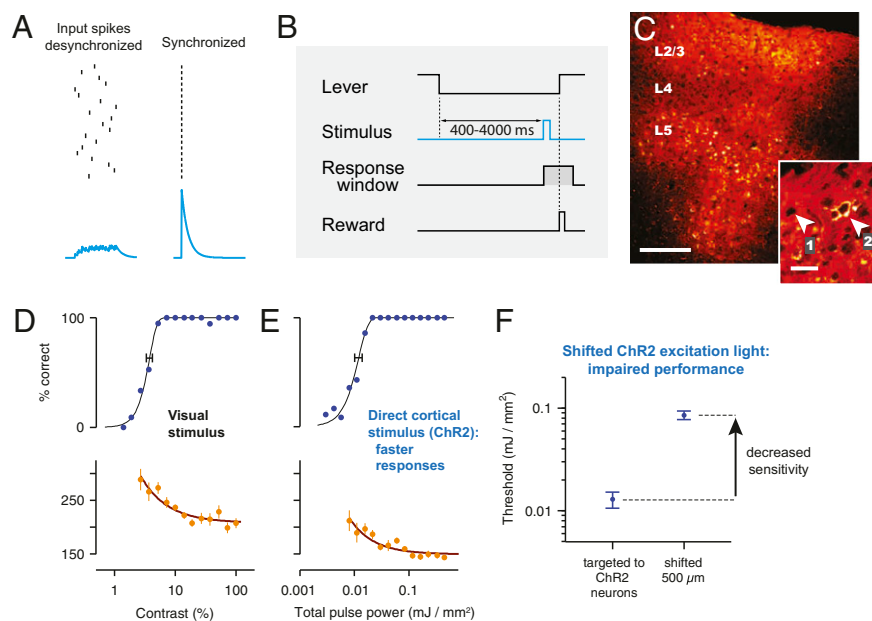


Fig. 1. Animals directly detect activation of cortical neurons by ChR2. (A) Schematic showing how spike synchrony among inputs affects input conductance. (Top) Simulated asynchronous (Left) or synchronous (Right) input spikes. (Bottom) Schematic of a conductance waveform that would result from summation of the same conductance response from each spike (convolution of spikes with an exponentially decaying response). (B) Change-detection behavior. Animals press a lever to initiate the trial, and after a random delay we deliver a light pulse to stimulate ChR2-expressing neurons. Animals respond by releasing the lever. Responses before the stimulus are false alarms; failures to release quickly (within 450 ms) are classified as misses. Correct releases are rewarded; errors cause the trial to end, and a delay is imposed before the next trial. (C) Histological section showing ChR2-expressing neurons, pseudocolored with yellow indicating highest fluorescence. The injection is a few hundred microns in diameter (see Fig. S1 for the distribution of responsive neurons). The area between neurons is densely labeled red because ChR2 is expressed in cell membranes throughout the neuropil. (Scale bar, 100 μm .) (Inset) Detailed view showing a cell with membrane expression (2) and one with less expression (1). (Scale bar, 20 μm .) (D and E) Typical behavioral sessions showing that animals are good psychophysical observers. (Upper) Psychometric functions. Horizontal black line: 95% CI for threshold. (Lower) Reaction times. Heavy lines are hyperbolic function fits; yellow points indicate means; error bars show SEM. At the highest stimulus intensity, reaction times are much shorter for direct cortical stimulation than for visual stimuli, because animals detect signals that bypass the sensory periphery. (F) Performance relies on optical excitation of ChR2 neurons, showing that animals detect changes in cortical activity and not retinal stimulation with blue light. The y axis shows the behavioral threshold (calculated as shown in D and E; 95% CIs). The left value shows the behavioral threshold when the excitation light spot is directed at ChR2 neurons; on the right, the elevated threshold reflects worse performance when the light spot is displaced $\sim 500 \mu\text{m}$ away from ChR2 expression peak ($n = 1$ animal, 15 behavioral sessions; see Fig. S2 for more details.).

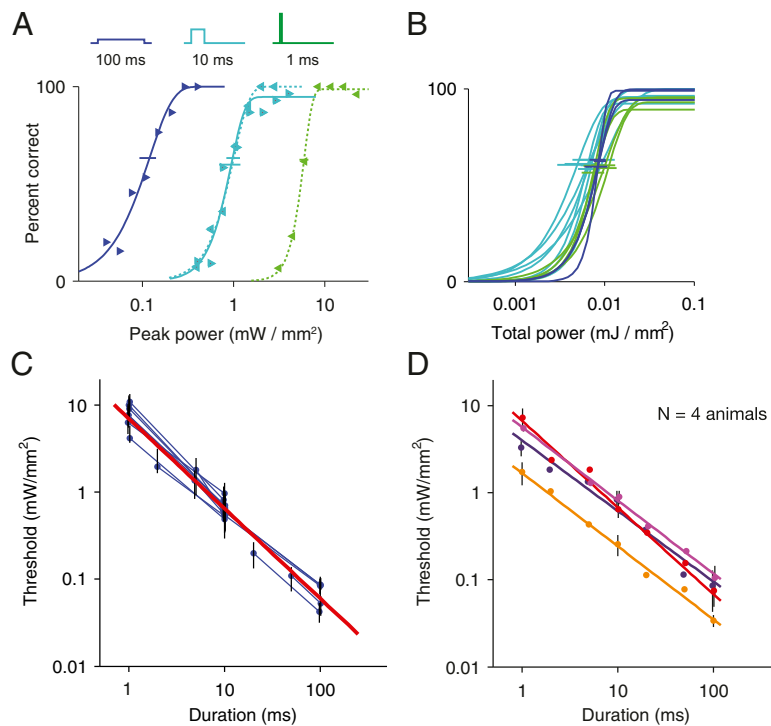


Fig. 2. Behavioral detection thresholds show that inputs can be integrated linearly. (A) An example of psychometric functions from two sessions in one animal. Dark blue, 100-ms pulse; cyan, 10-ms pulse; green, 1-ms pulse. Data shown in solid cyan and dark blue (single points shown with rightward-oriented triangles) were collected in one session; dotted cyan and green curves (leftward-oriented triangles) were obtained in a second session; within a session, trials were randomly intermixed. The x axis shows the peak power of each square pulse. Horizontal lines indicate the 95% CIs around each pulse duration's threshold. (B) An example of behavioral detection as a function of total pulse power. Data are from a second animal ($n = 10$ sessions.) The x axis shows total pulse power in millijoules per square millimeter, or peak power in milliwatts per square millimeter (as in A) times pulse duration in seconds. Other conventions are as in A. (C) The threshold is nearly linearly proportional to pulse time. Data are from the animal in B. Black points indicate threshold measurements for pulses of different durations (95% CI), slightly offset on the x axis for clarity. Blue lines connect pairs of measurements made in a single session (no normalization). The heavy red line indicates the linear fit; slope -1.01 . (D) Summary of data from four animals. Each color represents one animal (blue, animal with data in A; red, animal in B). Error bars at 1, 10, and 100 ms indicate the SEM. For each animal, data include at least five points at 1 and 100 ms and at least 10 points at 10 ms. Data are normalized to the threshold at either 10 ms or 100 ms, one of which was measured each day. Slope range: -0.85 to -1.01 . The slope measures animals' ability to integrate inputs; the offset on the y axis reflects only changes in absolute power threshold and could arise from many sources, including variation in dural thickness or slight differences in expression level (Fig. S2). Animals' lapse rates were low (median $<3\%$), and neither lapse rate nor slope varied with pulse duration (Fig. S7).

magnitude -1.00) and in terms of d' (slope on a log-log plot of duration vs. threshold d' : mean -0.89 , largest slope magnitude -1.15). This relationship, with a slope near -1 , means that the total light power (the product of pulse duration and amplitude) closely predicted behavioral performance (Fig. 2 B–D), whether the total power was distributed over 100 ms or was concentrated into an interval of only a few milliseconds. [We chose a minimum pulse length of 1 ms to fall just under the limits of ChR2 kinetics, because ChR2 has an activation time constant of 1.5 ms (29)]. This dependence on total power is unexpected for direct inputs to cortical neurons, because cortical neurons are variable and have nonlinearities caused by spike threshold and active dendrites. Such neuronal nonlinearities, if used in this behavior, would generate better performance for short pulses than for long pulses of the same total power. Instead, animals' behavior reflected nearly perfect linear integration.

To explore the neuronal basis of the linear behavioral integration we found, we first examined how neurons' firing was changed by optogenetic inputs. Our recordings during the task using a linearly changing light stimulus showed that neuronal firing rates varied monotonically with the ChR2 input (Fig. 3 A–C). We applied light stimuli both during and outside the detection task and found that spiking was similar in those two conditions (Fig. 3D). Therefore, to maximize statistical power, all further recordings we show are responses recorded outside the detection task while animals were

awake and receiving reward periodically to keep them alert. To determine if changes in spiking occurred with a time course similar to that of the light pulses we delivered, we next stimulated with square pulses and measured spiking in small neuronal populations. Consistent with ChR2 kinetic properties (activation time constant = 1.5 ms, deactivation time constant ~ 5 ms) (29), the duration of firing rate changes matched the duration of pulses. Higher-amplitude light pulses also produced larger changes in average firing rate (Fig. 3 E and F) or, equivalently, spike probability. (Below, we quantify these changes across a larger neuronal population.)

Population Firing Rates Change Linearly with both Pulse Duration and Amplitude. The simplest manifestation of the linearity we observed in behavior would be for the underlying neuronal population to show a linear relationship between input and spike output, despite individual neurons' threshold nonlinearities. In this case, the sum of population spike activity would be similar for short, high-amplitude and long, low-amplitude pulses over the ranges used for behavioral measurements. To test this case quantitatively, we recorded the activity of hundreds of units while stimulating with light in vivo (Fig. 4). For these studies we recorded many units ($n = 243$ single and multiunits responsive to stimulation; *Methods*), giving us the power to measure changes in spiking even at low light intensities near the behavioral threshold

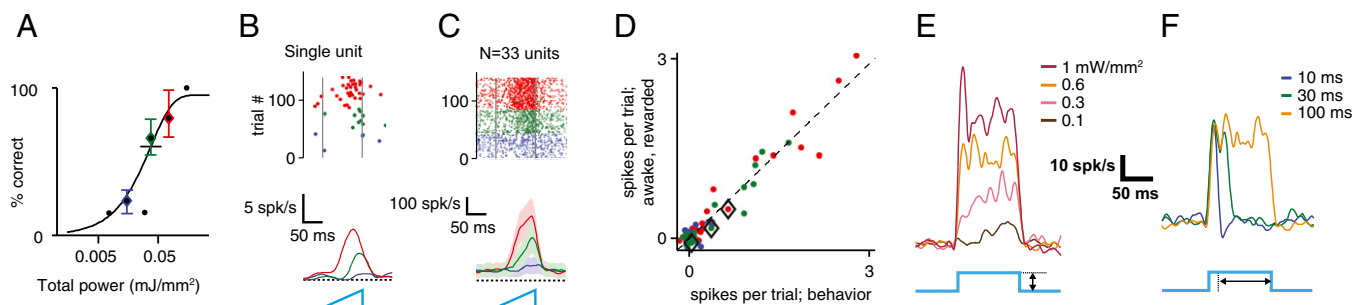


Fig. 3. ChR2 stimulation changes neuronal firing during behavior. (A) An example of psychometric behavioral performance, with three power levels highlighted: blue, below threshold; green, near threshold; and red, above threshold. Error bars: 95% binomial CIs. The x axis shows the total power for a 100-ms linear ramp; other conventions are as in Fig. 1 D and E. (B) Single-neuron response showing few spikes were fired per trial. (Upper) Raster; each dot is a spike. (Lower) Spike histograms showing probability of spiking over time. The single neuron fired 0.2 spikes per trial at a power slightly above threshold (green). (C) Population sum over 33 units (eight single and 25 multiunits) from one behavioral session. The activity in the population just above threshold (green) corresponds to an average of 0.23 extra spikes per recorded unit. (D) ChR2-evoked neuronal responses are similar during and outside the behavioral task. The x axis shows responses during behavior. The y axis shows responses while the animal was nonbehaving but awake and given occasional rewards (about one per minute) to maintain alertness. Each point is a single or multiunit at one power; powers are colored as in A; diamonds indicate data shown in B. (E and F) ChR2-evoked responses from a small neuronal population at powers above behavioral threshold. Data are mean responses over all units ($n = 19$; 5 single and 14 multiunits) from one recording session, collected from an awake animal (light yellow in Fig. 2D) outside behavior (see text and Fig. 4). (E) Spike responses increase as power is increased (pulse duration fixed at 100 ms). (F) Responses increase as pulse duration is increased (power fixed at 0.6 mW/mm^2).

(compared with Fig. 3 E and F, which used higher intensities). We found linear increases in spiking when the duration or amplitude of the stimulation pulse was increased (Fig. 4 A–D) and confirmed this finding by fitting a linear regression model containing terms for peak power, duration, and total power (peak power times duration). Only the total power term was significant ($P < 10^{-120}$), and it captured the entire effect; when the total power was accounted for, neither single factor modulated responses further ($P > 0.30$). The coefficient (β , or slope) of the total power term was 0.11; this is the number of spikes per cell per trial near behavioral threshold (Methods). We also observed linearity if we considered single units alone ($n = 53$; again, only the total power term was significant, $P < 10^{-25}$), where the coefficient is even smaller (0.050), as expected because multiunits group together several single units. The regression showed no distortions caused by changes in each variable alone, as might have occurred, for example, if short pulses had produced more spikes than long pulses of identical total power.

Instead, we found that the same number of spikes was generated by the population by pulses with the same total power (i.e., using higher peak powers for shorter pulses), even though shorter pulses yielded higher instantaneous firing rates (Fig. 4E). Stimulation with short pulses elevated the firing rate for only a few milliseconds at total powers near the behavioral threshold (Fig. 4E; a 3-ms light pulse elevated population activity for 4.4 ms, FWHM). Although responses could show slight initial transients at higher powers (e.g., Fig. 3E), these were not seen near the behavioral threshold (Fig. 4E), and even at high powers any transients were fast and caused little deviation from linearity (Fig. 4 A–D). Together, these observations support the idea that the total spike count over a 100-ms period is important for behavior, regardless of the maximum firing rate achieved or how those spikes (or the conductance inputs that cause them) are arranged in time.

The linear neuronal changes we observed might be possible because at low light powers ChR2 avoids nonlinearities such as desensitization and saturation. Experimental observations have shown that at low powers ChR2 exhibits a linear relationship between excitation light and channel conductance (29, 30), and this relationship has been quantified in biophysical models (29, 31), which we reimplemented to plot this linearity (Fig. 4F). Indeed, power densities at or above 10 mW/mm^2 applied directly

to a thin tissue section often are used to drive spiking in vitro (32); here we approach that number only for the shortest pulses, and we deliver power to the top of the dura, so that the light reaching cells is attenuated by overlying tissue. Therefore, the linearity of ChR2 at low light powers is likely to underlie the linearity we see between light intensity and our in vivo spike data. However, even in the presence of ChR2 linearity, the output spike count we measured would not be expected to be linear for short and long pulses of similar total power, because cellular nonlinearities such as threshold and active dendrites predict that short inputs should be more effective at driving spikes.

The low light levels needed for behavioral detection produced small changes in the firing rate of individual neurons (Fig. 5). The effects of ChR2 stimuli at the behavioral threshold were sufficiently weak so that neurons often fired no extra spikes on individual trials (mean: 0.11 extra spikes per unit per trial; SD: 0.26; equivalent to an average change in firing rate of 1.1 spike/s for a 100-ms stimulus; Fig. 5). As often seen in the cortex (33), the responses of neurons to stimulation were variable (noisy), following a nearly-Poisson distribution (Fano factor: mean 1.20) with a small but positive pairwise correlation (correlation coefficient: mean 0.016). The small rate changes and the Poisson trial-to-trial variability support the notion that we were activating only a fraction of the total ChR2 molecules (Fig. 4F), allowing ChR2 conductance to vary linearly with excitation light power. Although the ChR2 stimulus had only a small effect on individual neurons, many cells (both single and multiunits) showed these changes (Fig. 5). These data show that behavior in this task can be controlled by a population of many neurons, each of which changes its firing probability only slightly.

Periodic Pulse Trains Do Not Improve Detectability. The linear behavioral trade-off we found between pulse amplitude and duration suggests that periodic synchronization among inputs would not improve behavioral performance. To test this notion directly, we used pulsed light waveforms with different frequencies and pulse durations (Fig. 6 A–D). We held the length of each pulse train constant at 100 ms and varied the number of pulses from two to six, yielding frequencies between ~ 10 and 50 Hz. For trains with five pulses (45 Hz, near the middle of the gamma range), we also changed how tightly inputs were synchronized by varying

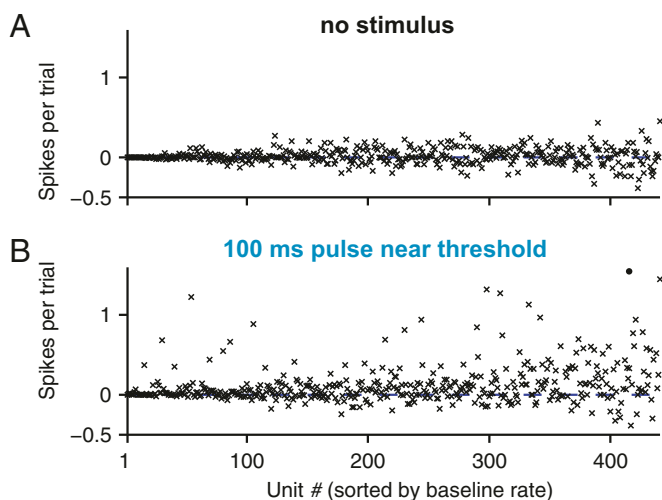


Fig. 5. Stimulation near the behavioral threshold produces small changes in the activity of many cells. Each point is the activity of one of 441 units (110 single, 331 multiunits) recorded from the same two animals shown in yellow and red in Fig. 2*D*. (*A*) Spike count in the absence of ChR2 stimulation, illustrating the size of our measurement noise (average over 90–110 repetitions). The y axis shows spike count in a 100-ms period with no stimulation, minus the count in a baseline period of the same duration. Each point is one unit, ordered (x axis) by mean absolute baseline firing rate (unit baselines: 10th percentile, 0.28 spikes/s; median, 2.8 spikes/s; 90th percentile, 9.9 spikes/s). (*B*) Spike counts in response to ChR2 stimulation at a power just above the behavioral threshold (0.1 mW/mm², 100-ms square pulse, 0.01 mJ/mm²). See Fig. S1 for spatial locations of recording sites. The single filled circle is a multiunit that fired 1.95 spikes per stimulus, shifted down to the axis limit for visual clarity. The mean response is 0.11 spikes per stimulus (an average change in rate of 1.1 spike/s over 100 ms), which is nearly identical to threshold found by the slope in Fig. 4*A* and *D*. These data were collected during the awake, rewarded condition (y axis, Fig. 3*D*) to maximize the number of trials and statistical power.

Discussion

Linear Population Codes Can Arise from Weak Inputs on a Noisy Background. We found that behavioral detection performance depends only on the number of spikes fired by a population over 100 ms, as if each spike were weighted equally, regardless of its arrival time. Also, although neuronal nonlinearities would predict that the total number of spikes should be amplified for short pulses, we instead observed linear population responses across a wide range of light pulse durations. How is it possible for behavior and neuronal spiking to vary linearly given the threshold and dendritic nonlinearities of single cells? The observations that behaviorally detectable inputs are weak and that individual cells are variable support a population coding model that can explain linear behavioral performance. Cortical neurons *in vivo* receive an ongoing barrage of input that produces large fluctuations in membrane potential and causes the cell to cross the threshold with highly irregular timing (11, 33, 34). The observed variability in the firing of cortical neurons generally is thought to arise from this background activity, because these neurons respond deterministically to input (35). Because small perturbations in nonlinear systems can produce linear responses (36), weak inputs added to the ongoing background fluctuations can change this probability of spiking slightly but linearly (18, 37). Thus, one important aspect of our findings is that small changes in firing rate over many neurons are behaviorally detectable.

However, the observation that small perturbations in the firing rate produce linearity is insufficient by itself to yield a population linear response, because the spike threshold rectifies neurons' input–output relationship. In principle, small inputs should have little or no effect on spiking, because they are insufficient to

cross threshold. This observation suggests that neurons act as coincidence detectors (12). However, background activity, which is largest in the cortex when animals are awake and alert (38) can explain how cortical neurons produce a linear population spike response. We observed that behaviorally detectable ChR2 input did not drive neurons to fire at high rates and did not produce reliable spiking (Fig. 5), showing that the ChR2 input rarely was sufficient by itself to cross the threshold. In the absence of ongoing cortical background input, these inputs likely would have produced few or no spikes, as is the case with the small excitatory postsynaptic potentials often generated by synaptic input (1, 39, 40). Instead, the observed trial-to-trial neuronal variability means that threshold crossings were determined primarily by background activity, and ChR2 inputs modify the chance of a spike firing only slightly. For single neurons it is difficult to discern such changes in firing probability on a single trial, but inputs can be decoded more reliably (by the animal or the experimenter) by summing spikes across a neuronal population (Fig. 4). In summary, the neuronal noise generated by ongoing activity may be a necessary nuisance that enables firing rate to vary linearly with input, avoiding the rectifying effects of spike threshold.

To guide a behavioral response from such a population of neurons that show small rate changes, many cells must participate in the population. Accordingly, we estimate that hundreds or thousands of neurons were stimulated by ChR2 during behavior. For the session shown as an example in Fig. 3*A–D*, we recorded 33 single and multiunits during behavior and saw 7.2 spikes per trial at threshold power (Fig. 3*C*, green). If we assume conservatively that each site can record from neurons up to 50 μ m away (41), we surveyed $\sim 1/25$ th of layer 2/3 of the injection site (Fig. 1*C*), so we would expect at least 150 spikes for each near-threshold stimulus. These recording electrodes were placed in the superficial cortical layers, and if neurons in deeper layers also were stimulated, we would expect even more spikes. Our data do not exclude the possibility that infrequent behavioral responses could be induced by far fewer spikes (Fig. 3*A–D*, blue) (10). However, as expected for a sum of variable Poisson spike counts, reliable behavioral performance (e.g., >50% correct) depends on the addition of many spikes to the population.

Over the wide ranges of duration and amplitude we measured, behavioral performance is predicted well by total integrated light power, with little advantage given to short pulses. This type of linear integration has been demonstrated behaviorally for brief visual, auditory, and other sensory stimuli, where it is called Bloch's law (42–44). This nearly perfect integration (slope near -1 on a log-log plot of threshold vs. duration; Fig. 2) has been thought to occur in the periphery, where graded potentials can support integration (42). Because cortical neurons are noisy and nonlinear, the linear integration we observed is unexpected for the direct conductance inputs we used. In studies of temporal integration over longer times, performance often improves with the square root of time [slope $-1/2$; (43)], rather than linearly with time (slope -1), as we find. However, temporal integration effects with slope $-1/2$ still can reflect perfect integration of sensory input (43, 45) when the stimuli involved vary randomly, so that performance is limited by statistical variations in the stimulus. However, because those statistically varying stimuli are suprathreshold and are easily visible, and because linearity for the dim, constant visual stimuli described by Bloch's law becomes imperfect beyond ~ 100 ms (42), studies of temporal integration over longer time periods might have a different neuronal circuit basis than our effects.

Generalization to Other Tasks and Areas. Different types of behavioral tasks might rely on different regimes of cortical computation and, unlike the effects we observed, might rely on the known nonlinearities in cortical neurons. We have studied how animals detect weak signals near the limits of perception. In other studies

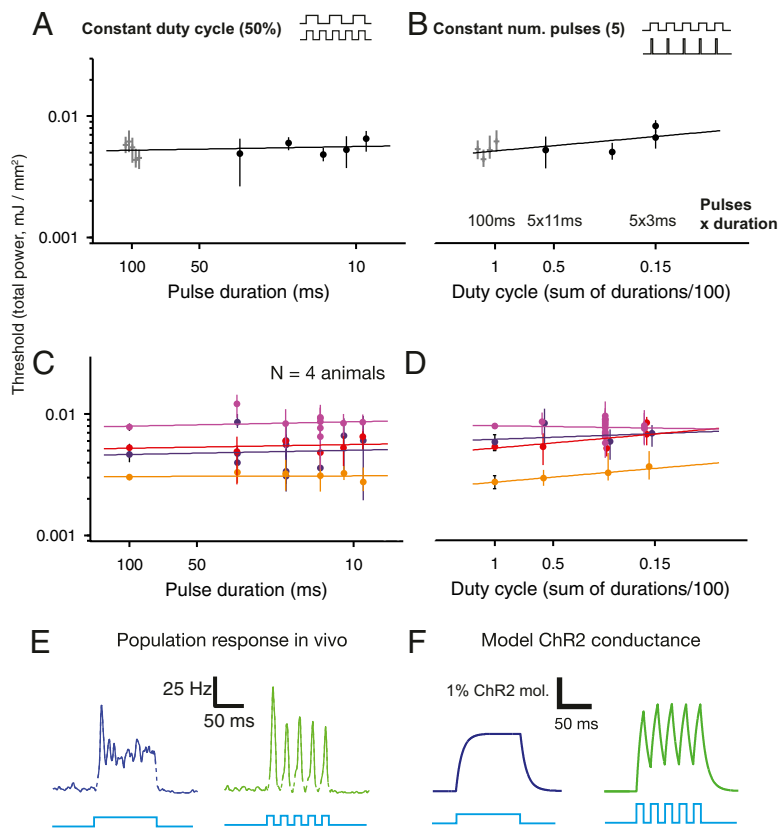


Fig. 6. Synchronization of inputs does not affect behavior over a wide range of frequencies. (A) Single-animal example for varying pulse duration with near-constant 50% duty cycle. (Slight deviations of duty cycle from 50% result because pulse durations always are multiples of 1 ms). The total train length is held constant at 100 ms, and the pulse number (and thus pulse duration, to keep 50% duty cycle) is varied. For example, the train with pulses of 20-ms duration has three 20-ms pulses (with two 20-ms gaps between them), resulting in a repetition frequency of 25 Hz. The train with pulses 11 ms in duration has five pulses (and four gaps) for a frequency of 45 Hz (schematic shown in *Inset*). The y axis shows the threshold (95% CI) in units of total integrated light intensity (mJ/mm², or mW/mm² times the sum of pulse durations for that train). As predicted by linear integration, different pulse durations give similar total power thresholds. The black line shows the linear fit. We additionally normalize each day's threshold measurement (black) by the ratio of that session's control 100-ms threshold (gray points, slightly offset horizontally for visual clarity) to the mean 100-ms threshold for that animal to reduce noise by slightly reducing session-to-session fluctuations in threshold (Fig. 2 C and D). (B) Data from a single animal showing the pulse duration while the number of pulses was held constant (all trains have five pulses with an 11-ms period, 45 Hz). The x axis shows the duty cycle, or total power as a fraction of the power of the 100-ms pulse. Other conventions are as in A. The slope is not significantly different from zero ($P > 0.05$), but any upward slope of the regression line would show that short pulses (of similar total power and thus higher amplitude) are less effective than long pulses at driving behavior, a result opposite that expected from cells' threshold nonlinearities. (C and D) Summary over four animals. Each color represents a different animal. Red data are for the animal shown in A and B; the animals and the colors are the same as in Fig. 2. Error bars: 95% CI, except for 100-ms control pulses: SEM. There is little variation in the behavioral threshold, as shown by near-zero slopes (no slope is significantly different from zero; $P > 0.05$ via linear regression, corrected for multiple comparisons). Upward trends in D suggest that short pulses may be even less effective in driving behavior at similar total power. (E) Responses in small populations (powers above behavioral threshold) verify that that pulsed stimulation evokes synchrony in cortical neurons; conventions are as in Fig. 3 E and F (average over $n = 19$ units, 5 single and 14 multiunits). (F) ChR2 model simulation shows that at low light levels conductance oscillations are limited by ChR2 kinetics, and there is substantial oscillation at 45 Hz, as we observed in vivo (E; also see Fig. 4E).

where animals have been asked instead to differentiate between two strong, suprathreshold patterns of activity generated by electrical microstimulation, they were able to detect differences in stimulus timing (46, 47). Electrical stimulation studies cannot examine network linearity, because pulsed current has a stronger effect than sustained current (48) and because there is a complex relationship between stimulation current and evoked spike count. However, the stimulation currents used likely evoked stronger activity than our near-threshold stimulation (27, 49). In fact, frequency discrimination of both sensory and direct electrical stimuli is best with intensities well above the detection threshold (50). Discrimination of two patterns thus might rely on more spikes in the population than detection of minimal stimulation. It remains unclear whether these stronger inputs and the computation they support take advantage of network nonlinearity.

Populations of nonlinear neurons may support linear temporal integration in brain regions beyond the visual cortex. On the one

hand, visual cortical neurons can show sustained sensory responses, but more transient responses, implying a stronger reliance on timing-based codes, have been observed in other primary sensory areas such as rodent somatosensory (barrel) and auditory cortex (51–53). However, in these other areas temporal integration is possible [e.g., when sensory stimuli are combined (51) and direct electrical stimuli are used (54)]. Across sensory cortical areas, there is strong divergence even in the first set of inputs, the thalamocortical connections, and most individual inputs are weak (1, 39, 55, 56). These are the conditions—when each cell receives many inputs and no single input dominates—under which population linearity can hold. Thus, it appears that other cortical areas have the anatomical capacity to produce such linear coding in some behavioral contexts. The fact that synchronized spiking in the V1 population (Fig. 6E) produced no behavioral advantage over sustained spiking (Fig. 6C) suggests

that the output of V1 was summed linearly by any stages that received that output and contributed to the behavioral response.

The cortical local field potential and EEG contain signatures of global oscillations in larger pools of neurons (6). Although a noisy population code explains why these oscillations need not impact behavior, inputs arriving at particular oscillation phases might be processed preferentially. If such phase-locking aided performance in our task, the pulsed waveforms sometimes would have arrived at the correct phase and sometimes would have arrived at the incorrect phase and thus should have increased the variability of reaction times and changed the slope of the psychometric function. We found no evidence for either effect (Fig. S5). Additionally, we observed no changes in pairwise synchrony amongst recorded neurons as a result of ChR2 stimulation (Fig. S6). Other computations might use this sort of synchrony, although coding via coherence between inputs and the local network state requires two distant neuronal populations to be synchronized with precise timing. Given the wide variety of axonal lengths and numbers of synapses between any two cortical neurons, each of which induce variable delays, the cortex might well have faced evolutionary pressure to develop coding schemes that are resistant to timing, such as those reflected in our data.

Conclusion

The linear behavior we observed is unexpected given the many nonlinearities at the cellular and network level that could have changed animals' behavior. At the single-cell level, spike threshold, active dendritic processes, or spike rate saturation and refractory periods could have changed the effect of coincident input. Known properties of cortical networks also could have produced nonlinearity, including excitatory recurrent amplification or damping by recruitment of inhibition, which indeed are known to occur under extreme conditions of strong input (57–59). Nonetheless, we find that recurrent cortical networks are capable of linear behavior. Likely requirements are that behaviorally relevant inputs are weak compared with other inputs (Fig. 5) and that inhibition roughly balances excitation (15, 16). Cortical circuits have corresponding anatomical features—specifically, dense, recurrent local excitatory connections and promiscuously connected inhibitory networks. Thus, the circuit architecture of the cortex may exist to allow such linear population coding.

Methods

Animals and Transfection. All animal procedures were approved by the Institutional Animal Care and Use Committee at Harvard Medical School and conformed to National Institute of Health guidelines. Adult animals (postnatal age 35 d or older; $n = 7$) were implanted with a head plate in aseptic surgery. Data from four animals are shown in Figs. 2 and 5; data from two of these animals are shown in Figs. 4 A–D, 5, and 6 E and F, and data from one of these animals is shown in Fig. 1E. Of the three remaining animals, data from one each are shown in Figs. 1D, 3 A–C, and 4E. Animals expressed an *Emx1*-Cre knock-in transgenic construct (Jackson Labs, stock #5628) and were outbred, derived mainly from C57/Bl6 and BALB/c lines. We injected an AAV2.8 virus into the binocular region of primary visual cortex (1 μ l over 40 min, $0.1\text{--}1 \times 10^9$ viral particles) containing ChR2 [the original variant without H134R mutation (60)] in a Cre-dependent inverted-floxed construct (61, 62) (FLIP/DIO) fused to mCherry.

ChR2 Stimulation. Several weeks after injection, we localized the area of maximum expression via wide-field fluorescence microscopy and fixed an optical fiber (400 μ m in diameter, 0.39 NA; Doric Lenses, Inc.) to the implant so that it terminated < 4 mm from the dural surface. We delivered light through the fiber via either a 473-nm low-noise solid-state laser (Laserglow, Inc.) for training and recording or via a 455-nm LED (for training only). We calibrated light intensity at the entrance to the cannula using a photodiode (Newport, Inc.) and measured insertion loss through each implanted fiber as ≤ 1 dB. The brain was covered by a glass optical window above agarose or a silicone adhesive (Kwik-sil; World Precision Instruments, Inc.), or by the adhesive alone. To calculate power density, we used a CCD camera to measure the laser spot size as the FWHM of intensity at the dural surface. Intensities at the dural

surface are an upper bound on intensities experienced by cells at depth because of loss in tissue and scattering (63), so our intensity measurements are difficult to compare across animals (e.g. the animal whose data is shown in Fig. 3 had a slightly higher detection threshold than other animals; this animal showed some tissue regrowth above the dura which may have attenuated stimulation light). Thus, we made only within-animal comparisons of intensity and collected each animal's behavioral data (Figs. 2 and 6) without disturbing the implant. To confirm that no threshold fluctuations occurred, we collected reference threshold data (for 100- or 10-ms pulses) during each session. We plot population data by normalizing to the reference (e.g., Fig. 2D) but omitting the normalization produced qualitatively identical results (compare Fig. 2 A–C).

Behavioral Task. Animals were trained to report changes in neuronal activity induced by ChR2 by manipulating a lever. We first trained animals to perform a task detecting visual changes (see ref. 23 for details) until they achieved a stable perceptual threshold. Then on all visual stimulation trials we added a 100-ms ChR2 stimulation pulse at 0.5–2 mW/mm² (5–10 times above the detection threshold) whose onset was simultaneous with the visual stimulus onset. Over one to eight sessions we made the visual task more difficult by progressively lowering contrast, making it increasingly advantageous for animals to use the ChR2 stimulus to guide behavior. When performance for all contrasts rose to nearly 100%, indicating that the animals were responding well to the ChR2 stimulus, we removed the visual stimulus. Over 5–10 sessions we gradually lowered the intensity of the ChR2 stimulus until we could estimate a perceptual threshold for a 100-ms ChR2 stimulus. All four animals (Figs. 2 and 6) that we trained to perform this task did so successfully and continued to perform the task well for several months. First we collected behavioral data for all animals for long (100-ms) pulses. We collected thresholds for shorter pulses later, ending with 1-ms pulses. The measurements for the pulse trains shown in Fig. 6 were made before short single pulses in two animals and after short single pulses in two animals; no differences were observed, and we observed no effects of learning for repeated measurements with the same pulse parameters over several sessions. For one animal we remeasured 100-ms pulse thresholds after collecting 1-ms pulse thresholds and found the 100-ms pulse thresholds had not changed, further indicating that learning did not affect our results. All stimulus parameters were interleaved randomly from trial to trial. We used threshold measurements only from sessions with > 200 total hits and misses, with low lapse rates at high intensities, and with a stable within-session false-alarm rate. (Fig. S7 shows that false-alarm distributions do not vary with pulse length.) Behavioral control was done with MWorks (<http://mworks-project.org>) and custom software in Matlab (The Mathworks) and Python (www.enthought.com).

Neuronal Recording. We recorded extracellularly from visual cortex using multi-site silicon probes (Neuronexus, Inc.; 32-site model $4 \times 8\text{--}100\text{--}400\text{--}177$ or 64-site model Buszaki64sp). Recording sites were 15 μ m in diameter. Some recording sites were treated to increase conductance by electrochemically depositing the conductive polymer PEDOT:PSS [poly(3,4-ethylenedioxythiophene): poly(styrenesulfonate)] (64) using the NanoZ (White Matter Research, Inc.). Recordings were targeted to the site of ChR2 expression by imaging mCherry fluorescence with a fluorescence microscope and camera (Zeiss, Inc). We modulated laser light intensity with a Pockels modulator (Conoptics, Inc.). If electrical artifacts due to intensity changes were present during recording, to prevent them we used a 1–2-ms linear ramp between intensities. We amplified site signals, filtered between 750 Hz and 7.5 kHz, and sampled around threshold crossings (Blackrock, Inc.). We sorted waveforms into single and multiunits by amplitude, shape, and interspike interval (OfflineSorter, Plexon, Inc.) independently on each site. We discarded threshold crossings during any laser pulse transition ramp (as indicated by broken lines in Fig. 5E) to remove any remaining artifacts. We recorded the spike data shown in Figs. 4 and 5 during the awake, rewarded condition (outside behavior while animals were awake and receiving occasional reward between light stimuli to keep them alert). Fig. 3 shows that these neuronal responses are similar to those during behavior.

Responsive units were defined as any that showed a significant change ($P < 0.05$, sign test, 120-ms response period compared with baseline) in response to ChR2 stimulation in the awake, rewarded condition. Baseline counts were computed on the same trials as response counts, and the two time periods were of matched duration; the baseline period ended 50 ms before the onset of stimulation. We pool single and multiunits together, because population analysis of single units alone produced similar effects. In fact, for measurements of spikes fired per stimulus, because we plot raw spike counts and do not normalize (Fig. 5), combining single neurons into multiunits only could have made our estimates larger and thus did not affect our conclusions.

Data in Figs. 4 A–D and 5 were recorded from two animals used for behavior (the animals shown by yellow and red lines in Fig. 2D). Data in Fig. 4E were recorded from an animal that had never been trained but was transfected with ChR2 as described above. Figs. 3 and 4 A–D include units responsive (as defined above, $n = 243/441$ units, 53 single and 190 multiunits) to pulses using a high fixed power to include cells that showed even small effects (1 mW/mm², 100-ms pulse; 0.1 mJ/mm²). Fig. 4E includes units responsive ($n = 75/105$, 26 single and 49 multiunits) at the single fixed total power we used (0.005 mJ/mm²), pooling over pulse duration. We used responsive neurons in Fig. 4 A–E because averaging only over cells that showed a response is appropriate when computing response size per cell. However, using all cells had no qualitative effects on the results and only decreased the number of spikes fired per cell per trial; including all cells thus would have made our small modulation estimates even smaller. Responses from the entire Fig. 4 A–D dataset are shown in Fig. 5 and Fig. S1 ($n = 441$, 110 single and 331 multiunits).

Behavioral Data Analysis. Psychometric data were fit to mean responses with Weibull cumulative density functions via least-squares weighted by the variance of each mean [weighting by variance reduces bootstrap variance and improves fit (65)]. Thresholds are the Weibull location parameter: the 63% point between upper and lower asymptotes. To control for fluctuations in percent correct that might be induced by changes in the animal's willingness to respond, or criterion (66), we applied a correction to hit rate based on signal detection principles as described in ref. 23. We estimated the probability that each correct response was a guess or a spurious correct, based on the reaction time window and time-dependent false-alarm rate at each point in the trial and subtracted a proportionate number of correct trials. This correction brings the hit rate to zero for the lowest intensities. However, because false-alarm rates were not high, and we presented stimuli at various times within the trial, the overall frequency of spurious corrects resulting from guessing was low before correction for even the lowest intensities (maximum correction: 12%; median: <5%). Even without the correction, we observed no differences in criterion (false-alarm rate; Fig. S7) across pulse durations, and normalizing by a second threshold, estimated on intermixed trials to control for criterion, did not change our results (Fig. 2 C and D). We used least-squares optimization to estimate the lapse rate (upper asymptote), slope, and location parameters and fixed the lower asymptote at 0% correct (because of the above correction). Confidence intervals (CIs) for threshold were estimated via nonparametric bootstrap (67). Fits and CIs were estimated separately for both types of trials (10/100 ms control, or varying pulse pattern) within session. To control further for any potential criterion fluctuations, we calculated threshold in terms of d' (66). We found the probability of false alarm, given no response or stimulus had

yet occurred, as a function of time within trial in 50-ms bins. We observed this probability was constant with trial duration, so we averaged over durations and scaled by the length of the reaction time window to produce two false-alarm rates per session, one for each randomly intermixed pulse duration. We found d' for each stimulus intensity as $\Phi^{-1}(H) - \Phi^{-1}(FA)$, where Φ^{-1} is the inverse of the cumulative Gaussian distribution, H is hit rate or (uncorrected) percent correct, and FA is the false-alarm rate. In accordance with ref. 68, we fit a Naka–Rushton equation to the d' values and extracted threshold as c_{50} . We then used linear regression on \log_{10} -transformed duration and threshold to find the slope for each animal, and, as expected from the similarity of false-alarm rates, we found near-linear scaling, as when computing threshold with corrected percent correct (Results and Fig. 2).

Neuronal Data Analysis. Histograms were smoothed using a piecewise-regressive (Lowess) method. We used a multiple linear regression to determine whether spike count varied linearly with the product of power and duration. The regression independent variable was the mean count above baseline for each cell over a 120-ms period after stimulation; dependent terms were power, duration, and power times duration (total power). A constant term was included in the model but explains no variance because baseline subtraction yields zero spikes in the absence of stimulation. So that the coefficient (β) could be interpreted directly as the mean number of spikes at threshold (0.11), in the regression we normalized the total power term (power times duration) by the average total power at threshold over animals (Fig. 4). For the 3D plots in Fig. 4 C and D, we dropped any measurements with a mean rate below 0.02 spikes/s, because 90–110 measurements did not produce reliable estimates for these low rates; this rate was below the behavioral detection threshold of 0.11 spikes/s. To determine if ChR2 conductance varied linearly with light duration and amplitude, we implemented the four-state ChR2 biophysical model of Nikolic et al. (29, 31). Simulations confirmed that, at low light levels, neither desensitization nor saturation causes nonlinearities (Fig. 4F). We also found that ChR2 kinetics were not limiting; the maximum frequencies we used produce significant oscillation in ChR2 conductance (Figs. 4F and 5F; see ref. 69). Data were analyzed and simulations implemented with Matlab and Python.

ACKNOWLEDGMENTS. We thank Andrew McKinney, Amalie Thavikulwat, Alex Handler, and Steven Sleboda for help with behavioral training and analysis; Lindsey Glickfeld, John Assad, Chris Harvey, Tim Vogels, Marge Livingstone, Patrick Mayo, Nicole Comfort, and Incheol Kang for discussions and comments on the manuscript; and Tim Blanche and Tim Harris for discussions about PEDOT:PSS deposition. Funding was provided by the Howard Hughes Medical Institute.

- Bruno RM, Sakmann B (2006) Cortex is driven by weak but synchronously active thalamocortical synapses. *Science* 312(5780):1622–1627.
- Steriade M (2001) Impact of network activities on neuronal properties in corticothalamic systems. *J Neurophysiol* 86(1):1–39.
- Sjöström PJ, Rancz EA, Roth A, Häusser M (2008) Dendritic excitability and synaptic plasticity. *Physiol Rev* 88(2):769–840.
- Xu NL, et al. (2012) Nonlinear dendritic integration of sensory and motor input during an active sensing task. *Nature* 492(7428):247–251.
- Palmer LM, et al. (2012) The cellular basis of GABA(B)-mediated interhemispheric inhibition. *Science* 335(6071):989–993.
- Fries P (2005) A mechanism for cognitive dynamics: Neuronal communication through neuronal coherence. *Trends Cogn Sci* 9(10):474–480.
- Isomura Y, et al. (2006) Integration and segregation of activity in entorhinal-hippocampal subregions by neocortical slow oscillations. *Neuron* 52(5):871–882.
- Lefort S, Tomm C, Floyd Sarria J-C, Petersen CCH (2009) The excitatory neuronal network of the C2 barrel column in mouse primary somatosensory cortex. *Neuron* 61(2):301–316.
- Brecht M, Schneider M, Sakmann B, Margrie TW (2004) Whisker movements evoked by stimulation of single pyramidal cells in rat motor cortex. *Nature* 427(6976):704–710.
- Houweling AR, Brecht M (2008) Behavioural report of single neuron stimulation in somatosensory cortex. *Nature* 451(7174):65–68.
- Abeles M (1991) *Corticonics: Neural Circuits of the Cerebral Cortex* (Cambridge Univ Press, Cambridge, UK).
- König P, Engel AK, Singer W (1996) Integrator or coincidence detector? The role of the cortical neuron revisited. *Trends Neurosci* 19(4):130–137.
- Long MA, Fee MS (2008) Using temperature to analyse temporal dynamics in the songbird motor pathway. *Nature* 456(7219):189–194.
- Long MA, Jin DZ, Fee MS (2010) Support for a synaptic chain model of neuronal sequence generation. *Nature* 468(7322):394–399.
- van Vreeswijk C, Sompolinsky H (1996) Chaos in neuronal networks with balanced excitatory and inhibitory activity. *Science* 274(5293):1724–1726.
- Shadlen MN, Newsome WT (1998) The variable discharge of cortical neurons: Implications for connectivity, computation, and information coding. *J Neurosci* 18(10):3870–3896.
- Shadlen, M.N, Movshon, J.A (1999) Synchrony unbound: A critical evaluation of the temporal binding hypothesis. *Neuron* 24(1):67–77.
- Reid RC (2001) Divergence and convergence: Multielectrode analysis of feedforward connections in the visual system. *Prog Brain Res* 130:141–154.
- London M, Roth A, Beeren L, Häusser M, Latham PE (2010) Sensitivity to perturbations in vivo implies high noise and suggests rate coding in cortex. *Nature* 466(7302):123–127.
- Hubel DH, Wiesel TN (1959) Receptive fields of single neurones in the cat's striate cortex. *J Physiol* 148:574–591.
- DeAngelis GC, Ohzawa I, Freeman RD (1993) Spatiotemporal organization of simple-cell receptive fields in the cat's striate cortex. II. Linearity of temporal and spatial summation. *J Neurophysiol* 69(4):1118–1135.
- Bonin V, Histed MH, Yurgenson S, Reid RC (2011) Local diversity and fine-scale organization of receptive fields in mouse visual cortex. *J Neurosci* 31(50):18506–18521.
- Histed MH, Carvalho LA, Maunsell JHR (2012) Psychophysical measurement of contrast sensitivity in the behaving mouse. *J Neurophysiol* 107(3):758–765.
- Doty RW (1969) Electrical stimulation of the brain in behavioral context. *Annu Rev Psychol* 20:289–320.
- Huber D, et al. (2008) Sparse optical microstimulation in barrel cortex drives learned behaviour in freely moving mice. *Nature* 451(7174):61–64.
- Murphy DK, Maunsell JHR (2007) Behavioral detection of electrical microstimulation in different cortical visual areas. *Curr Biol* 17(10):862–867.
- Histed MH, Ni AM, Maunsell JHR (2013) Insights into cortical mechanisms of behavior from microstimulation experiments. *Prog Neurobiol* 103:115–130.
- Choi GB, et al. (2011) Driving opposing behaviors with ensembles of piriform neurons. *Cell* 146(6):1004–1015.
- Nikolic K, et al. (2009) Photocycles of channelrhodopsin-2. *Photochem Photobiol* 85(1):400–411.
- Lin JY, Lin MZ, Steinbach P, Tsien RY (2009) Characterization of engineered channelrhodopsin variants with improved properties and kinetics. *Biophys J* 96(5):1803–1814.

31. Grossman N, Nikolic K, Toumazou C, Degenaar P (2011) Modeling study of the light stimulation of a neuron cell with channelrhodopsin-2 mutants. *IEEE Trans Biomed Eng* 58(6):1742–1751.
32. Boyden ES, Zhang F, Bamberg E, Nagel G, Deisseroth K (2005) Millisecond-timescale, genetically targeted optical control of neural activity. *Nat Neurosci* 8(9):1263–1268.
33. Tolhurst DJ, Movshon JA, Dean AF (1983) The statistical reliability of signals in single neurons in cat and monkey visual cortex. *Vision Res* 23(8):775–785.
34. Destexhe A, Paré D (1999) Impact of network activity on the integrative properties of neocortical pyramidal neurons in vivo. *J Neurophysiol* 81(4):1531–1547.
35. Mainen ZF, Sejnowski TJ (1995) Reliability of spike timing in neocortical neurons. *Science* 268(5216):1503–1506.
36. Strogatz SH (1994) *Nonlinear Dynamics and Chaos* (Addison-Wesley, Reading, MA).
37. Anderson JS, Lampl I, Gillespie DC, Ferster D (2000) The contribution of noise to contrast invariance of orientation tuning in cat visual cortex. *Science* 290(5498):1968–1972.
38. Steriade M, Timofeev I, Grenier F (2001) Natural waking and sleep states: A view from inside neocortical neurons. *J Neurophysiol* 85(5):1969–1985.
39. Alonso JM, Usrey WM, Reid RC (2001) Rules of connectivity between geniculate cells and simple cells in cat primary visual cortex. *J Neurosci* 21(11):4002–4015.
40. Ts'o DY, Gilbert CD, Wiesel TN (1986) Relationships between horizontal interactions and functional architecture in cat striate cortex as revealed by cross-correlation analysis. *J Neurosci* 6(4):1160–1170.
41. Hetherington PA, Swindale NV (1999) Receptive field and orientation scatter studied by tetrode recordings in cat area 17. *Vis Neurosci* 16(4):637–652.
42. Barlow HB (1958) Temporal and spatial summation in human vision at different background intensities. *J Physiol* 141(2):337–350.
43. Palmer J, Huk AC, Shadlen MN (2005) The effect of stimulus strength on the speed and accuracy of a perceptual decision. *J Vis* 5(5):376–404.
44. Recanzone GH, Sutter ML (2008) The biological basis of audition. *Annu Rev Psychol* 59:119–142.
45. Brunton BW, Botvinick MM, Brody CD (2013) Rats and humans can optimally accumulate evidence for decision-making. *Science* 340(6128):95–98.
46. Romo R, de Lafuente V (2013) Conversion of sensory signals into perceptual decisions. *Prog Neurobiol* 103:41–75.
47. Yang Y, Zador AM (2012) Differences in sensitivity to neural timing among cortical areas. *J Neurosci* 32(43):15142–15147.
48. Rattay F (1986) Analysis of models for external stimulation of axons. *IEEE Trans Biomed Eng* 33(10):974–977.
49. Histed MH, Bonin V, Reid RC (2009) Direct activation of sparse, distributed populations of cortical neurons by electrical microstimulation. *Neuron* 63(4):508–522.
50. Romo R, Hernández A, Zainos A, Salinas E (1998) Somatosensory discrimination based on cortical microstimulation. *Nature* 392(6674):387–390.
51. Simons DJ (1985) Temporal and spatial integration in the rat SI vibrissa cortex. *J Neurophysiol* 54(3):615–635.
52. Stüttgen MC, Schwarz C (2010) Integration of vibrotactile signals for whisker-related perception in rats is governed by short time constants: Comparison of neurometric and psychometric detection performance. *J Neurosci* 30(6):2060–2069.
53. Wehr M, Zador AM (2003) Balanced inhibition underlies tuning and sharpens spike timing in auditory cortex. *Nature* 426(6965):442–446.
54. Butovas S, Schwarz C (2007) Detection psychophysics of intracortical microstimulation in rat primary somatosensory cortex. *Eur J Neurosci* 25(7):2161–2169.
55. Peters A, Payne BR (1993) Numerical relationships between geniculocortical afferents and pyramidal cell modules in cat primary visual cortex. *Cereb Cortex* 3(1):69–78.
56. Binzegger T, Douglas RJ, Martin KAC (2009) Topology and dynamics of the canonical circuit of cat V1. *Neural Netw* 22(8):1071–1078.
57. Creutzfeldt OD, Watanabe S, Lux HD (1966) Relations between EEG phenomena and potentials of single cortical cells. I. Evoked responses after thalamic and epicortical stimulation. *Electroencephalogr Clin Neurophysiol* 20(1):1–18.
58. Goddard GV, McIntyre DC, Leech CK (1969) A permanent change in brain function resulting from daily electrical stimulation. *Exp Neurol* 25(3):295–330.
59. Chung S, Ferster D (1998) Strength and orientation tuning of the thalamic input to simple cells revealed by electrically evoked cortical suppression. *Neuron* 20(6):1177–1189.
60. Nagel G, et al. (2003) Channelrhodopsin-2, a directly light-gated cation-selective membrane channel. *Proc Natl Acad Sci USA* 100(24):13940–13945.
61. Cardin JA, et al. (2009) Driving fast-spiking cells induces gamma rhythm and controls sensory responses. *Nature* 459(7247):663–667.
62. Sohal VS, Zhang F, Yizhar O, Deisseroth K (2009) Parvalbumin neurons and gamma rhythms enhance cortical circuit performance. *Nature* 459(7247):698–702.
63. Madisen L, et al. (2012) A toolbox of Cre-dependent optogenetic transgenic mice for light-induced activation and silencing. *Nat Neurosci* 15(5):793–802.
64. Xiao Y, Martin DC, Cui X, Shenai M (2006) Surface modification of neural probes with conducting polymer poly(hydroxymethylated-3,4- ethylenedioxythiophene) and its biocompatibility. *Appl Biochem Biotechnol* 128(2):117–130.
65. Wichmann FA, Hill NJ (2001) The psychometric function: II. Bootstrap-based confidence intervals and sampling. *Percept Psychophys* 63(8):1314–1329.
66. Green DM, Swets JA (1966) *Signal Detection Theory and Psychophysics* (Robert E. Krieger, Huntington, NY).
67. Wichmann FA, Hill NJ (2001) The psychometric function: I. Fitting, sampling, and goodness of fit. *Percept Psychophys* 63(8):1293–1313.
68. Herrmann K, Heeger DJ, Carrasco M (2012) Feature-based attention enhances performance by increasing response gain. *Vision Res* 74:10–20, 10.1016/j.visres.2012.04.016.
69. Crowley JJ, Fioravante D, Regehr WG (2009) Dynamics of fast and slow inhibition from cerebellar golgi cells allow flexible control of synaptic integration. *Neuron* 63(6):843–853.

Supporting Information

Histed and Maunsell 10.1073/pnas.1318750111

SI Methods

Data Analysis. To compute reaction times at threshold, we linearly interpolated between reaction times at the sampled powers, because the threshold typically fell between two presented light power levels. Because reaction times can be measured only on correct trials, we excluded power levels when the percent correct was less than 40%.

Illumination Spot and mCherry Fluorescence Measurements. The illumination spot area was defined as the area bounded by the half-maximum fluorescence level. To measure this area, we imaged the illumination of the cortex with a fluorescence microscope when excitation light was delivered through the fixed fiber, ensuring

that no pixels were saturated. We smoothed the resulting image with a 2D Gaussian filter, $\sigma = 5 \mu\text{m}$, and found the contour line at 50% intensity between background and maximum. This contour line is the boundary of the blue areas shown in Fig. S2. The mCherry fluorescence image and intensity contours labeled in Fig. S2 were computed similarly by imaging the emitted red fluorescence and smoothing to find contours. To find the average fluorescence in each illumination spot, we computed the mean mCherry fluorescence value, normalized so that background was 0% and maximum intensity 100%, for all pixels inside the half-maximum illumination spot boundary. The two illumination spots resulted from two different implanted fibers.

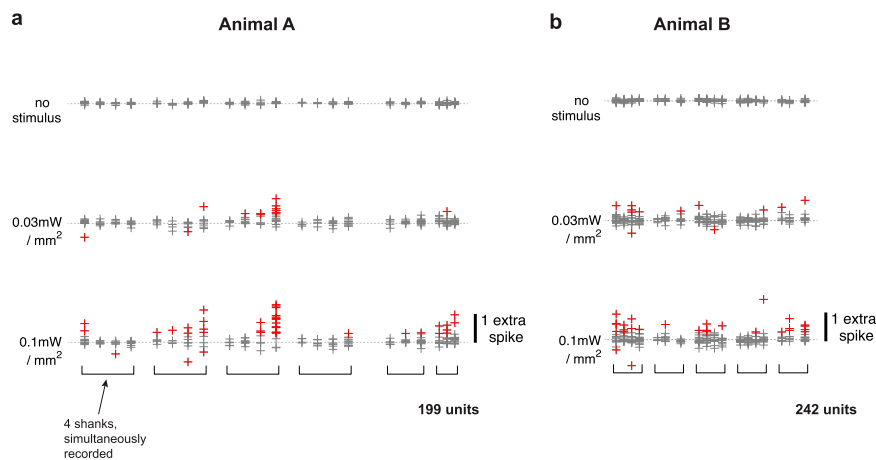


Fig. S1. Neural responses across recording sessions. (A and B) We recorded 441 single units and multiunits from two animals outside the behavioral task. We found that each unit was modulated only weakly near the behavioral threshold, implying that behavior is controlled by a population of neurons that fires a spike infrequently on each trial (Fig. 4). These data are summarized for the two animals. The rows show different stimulation powers (all using 100-ms pulses). *Top*, no stimulus; two baseline periods are subtracted to indicate our measurement noise. Plus symbols indicate the mean response for each unit across 90–110 stimulus repetitions (y axis: average spike number per trial during pulse compared with a same-duration baseline period ending 50 ms before pulse; see *Methods*). Responses greater than 0.3 extra spikes per trial are shown in red. We show extra spikes produced in response to stimulation without normalizing; thus, grouping single neurons into multiunit recordings could only increase the number of extra spikes. Because we find that each unit fires few spikes, we plot single and multiunits together. (In Fig. 5 in the main text, we plot each unit's response, ordered by each unit's baseline activity, again showing that both single and multiunits fire few spikes.) All units collected on a single shank are plotted at the same location (40 total shanks). Multisite silicon probes had four shanks, separated by either 400 μm (left-most columns, animal A) or 200 μm (all columns, animal B). Horizontal brackets in the bottom row connect all shanks recorded simultaneously. The electrode position was targeted to the area of maximum fluorescence but was different for each recording session. Behavioral thresholds for these animals (yellow and red lines in Fig. 2) are 0.036 mW/mm^2 and 0.065 mW/mm^2 , between the powers shown in the middle and bottom rows. These data show that channelrhodopsin-2 (ChR2) responses can be observed from shanks separated by at least 400 μm . Responding neurons thus are distributed across several hundred microns of the cortex, similar to the cells activated by a minimal visual stimulus, because of receptive field size and scatter (1) as in primates (2). This result confirms our anatomical observations; we found ChR2-expressing neurons (Fig. 1E) to be distributed over a cortical region a few hundred microns in diameter.

1. Bonin V, Histed MH, Yurgenson S, Reid RC (2011) Local diversity and fine-scale organization of receptive fields in mouse visual cortex. *J Neurosci* 31(50):18506–18521.
2. Dow BM, Snyder AZ, Vautin RG, Bauer R (1981) Magnification factor and receptive field size in foveal striate cortex of the monkey. *Exp Brain Res* 44(2):213–228.

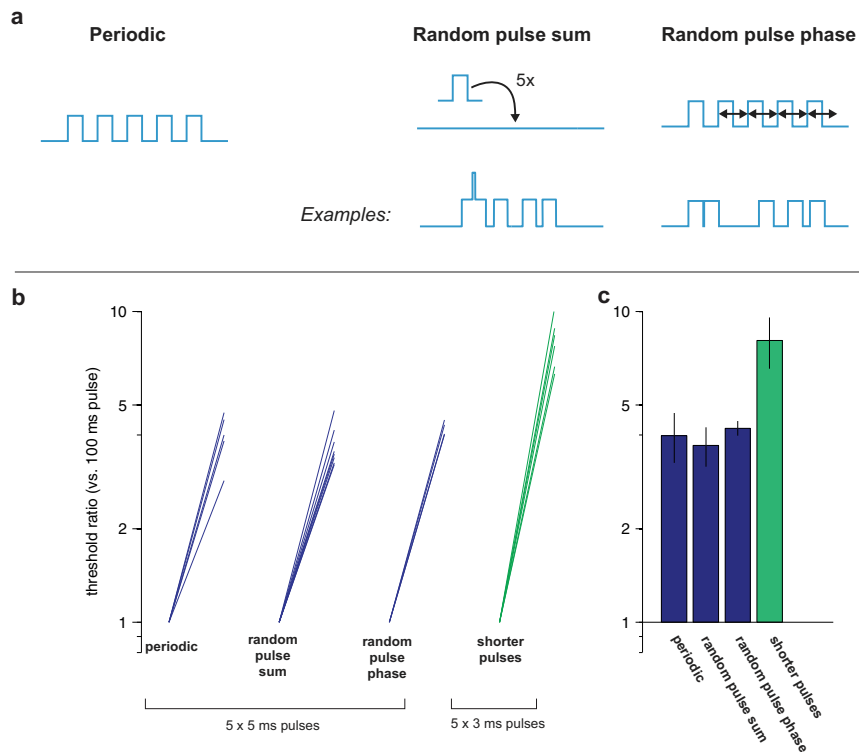


Fig. S3. Randomizing pulses within trains does not affect behavior. In principle, synchrony and short pulses could produce offsetting effects, although biophysical facts suggest both should produce the same direction of effect on behavior. To rule out the possibility of offsetting effects directly, we measured behavioral thresholds while varying pulse position within the pulse train. We performed this randomization in two ways. (A) (Left) We generated trains by starting with a blank 100-ms interval and dropping five pulses (each 5 ms in duration) uniformly onto the interval, allowing them to sum if they overlapped (Center: random pulse sum). (Right) Then, starting with a periodic train, we uniformly shifted each pulse within a single period (random pulse phase). We generated a different random train for each trial. Randomizing pulse trains had no effect on behavioral threshold. (B) Thresholds: For each measurement, we obtained curves for 100-ms control pulses and the pulse trains. Lines connect the two thresholds measured on each day. We divided both by the 100-ms control threshold so the control threshold was set to 1 (y axis). Because each pulse train had five pulses of 5 ms (integral = 25 ms, or 0.25 times the 100-ms pulse), measured thresholds were four times higher, as expected. There was no difference in threshold for randomizing the pulse sum or phase, as summarized in C (bar height shows the threshold mean, and error bars show the SEM). For comparison we show thresholds for five periodic pulses of 3 ms (green) [the same period as 5×5 ms (periodic, Left)], 22 ms, or 45 Hz. These thresholds are elevated, as expected when behavior is affected only by total input and not by its temporal pattern. Shown are random pulse data from 12 sessions, one animal; 5×5 and 5×3 ms data are from 11 sessions across four animals as in Fig. 6.

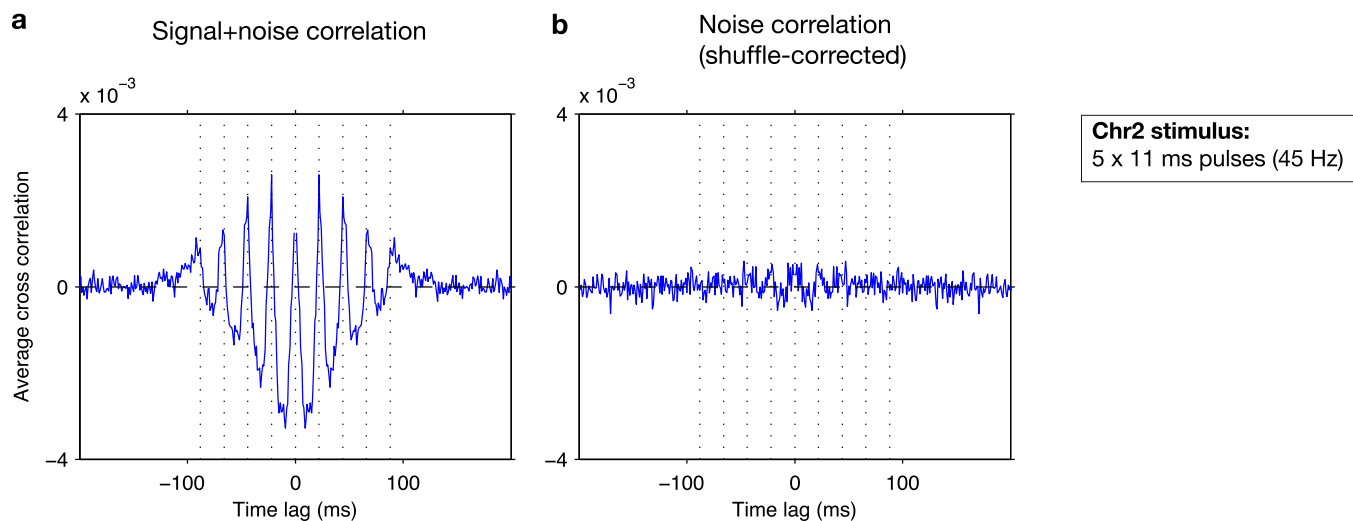


Fig. 56. Changes in neural cross-correlation are primarily signal correlations, arising from rate changes caused by light stimulation. (A) Average cross-correlogram over 5,886 simultaneously recorded pairs to trains of five square pulses, each 11 ms long (22-ms period; 45 Hz). The dotted lines indicate the lag corresponding to the middle of each stimulation pulse. The y axis shows the correlation normalized by variance so that auto-correlation is 1 at lag 0. Cross-correlation in response to 100-ms pulses has been subtracted to remove baseline slow shifts caused by the stimulation envelope. The lag = 0 point has been removed to ensure there is no contamination from light artifact. (B) The data in A have been shuffle-corrected (trial identity has been shuffled randomly for each pair to give an estimate of signal correlation only, and this estimate has been subtracted). The result is the noise correlation only, the change in pairwise correlation that comes not from the stimulus but from trial-by-trial variations in the network. All data are from four recording sessions in two animals; to measure these correlations, we presented 90-110 repetitions of pulse train stimuli. Single and multiunits are pooled. The pairwise signal correlation (A) is much larger than any noise correlation (B), showing that the primary effect of Chr2 stimulation is to change neurons' rate (i.e., the correlation with the stimulus; signal correlation), and not their correlation with each other (noise correlation). This result was expected, because we observed that neurons were near-Poisson with small positive pairwise correlation. Chr2 stimulation perturbs each neuron only slightly compared with background fluctuations, so its effect on global network coupling can be small; the primary effect is to encode the input in a small but linear change in spike probability.

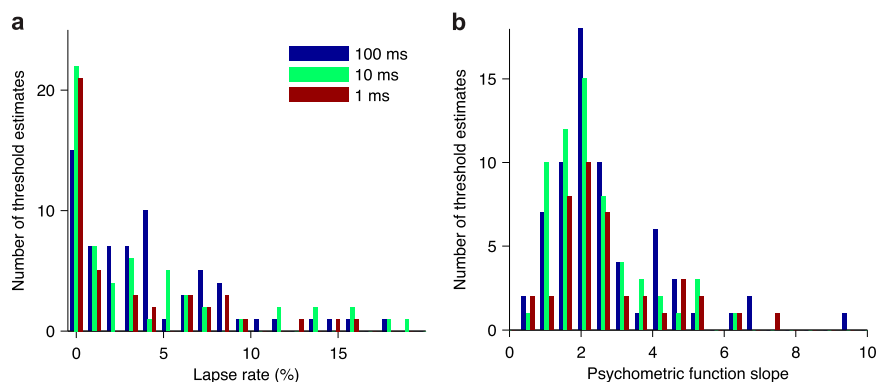


Fig. 57. The lapse rate and the slope of the psychometric function do not vary with pulse duration. For psychometric measurements using single pulses of varying duration (shown in Fig. 2), we plot above the lapse rate (deviation from 100% performance for the easiest high-power conditions) and psychometric function slope (data from four animals). Lapse rate: $100 - c_{\text{upper}}$, where c_{upper} is the upper asymptote of the fitted Weibull function (*Methods*). The slope is the Weibull β parameter. (A) Lapse rate histogram. Blue, 100-ms pulse; green, 10-ms pulse; red, 1-ms pulse. Medians are 3.9%, 3.0%, and 1.2%, respectively; differences are not statistically significant; all pairwise P values > 0.05 ; Wilcoxon test. (B) Slope histogram; conventions as in A. Medians are 2.6, 2.3, and 2.7, respectively; differences are not statistically significant; all pairwise P values > 0.05 ; Wilcoxon test). There was no systematic change in either lapse rate or slope as a function of light pulse duration.